



Contents lists available at SCCE

Journal of Soft Computing in Civil Engineering

Journal homepage: www.jsoftcivil.com



An Interior-Constraint BEM for Regularization of Problems with Improper Boundary Conditions

G.F. Mathews¹, D.C. Rizos^{2*} , R.L. Mullen³

1. Assistant Professor, Department of Civil Engineering, Penn State Harrisburg, Middletown, PA 17057, USA

2. Associate Professor, Department of Civil and Environmental Engineering, University of South Carolina, Columbia, SC 29208, USA

3. Professor, Department of Civil and Environmental Engineering, University of South Carolina, Columbia, SC 29208, USA

Corresponding author: rizos@engr.sc.edu

 <https://doi.org/10.22115/SCCE.2018.108597.1036>

ARTICLE INFO

Article history:

Received: 28 November 2017

Revised: 11 January 2018

Accepted: 11 January 2018

Keywords:

Boundary element method;
Rigid body motion constrains;
Regularization;
Approximate solutions.

ABSTRACT

A well-posed problem in the analysis of elastic bodies requires the definition of appropriate constraints of the boundary to prevent rigid body motion. However, one is sometimes presented with the problem of non-self-equilibrated tractions on an elastic body that will cause rigid body motion, while the boundary should remain unconstrained. One such case is the analysis of multi-particle dynamics where the solution is obtained in a quasi-static approach. In such cases, the motion of the particles is governed by the dynamic equilibrium while the contact forces between particles may be computed from elastostatic solutions. This paper presents two regularization methods of Interior-Constraint Boundary Element techniques for elastostatic analysis with improper boundary supports. In the proposed method rigid body modes are eliminated by imposing constraints on the interior of an elastic body. This is accomplished through simultaneously solving the governing Boundary Integral Equation and Somigliana's Identity. The proposed method is examined through assessment and verification studies where it is demonstrated, that for all considered problems rigid body motion is successfully constrained with minimal effects on body deformations.

How to cite this article: Mathews GF, Rizos DC, Mullen RL. An interior-constraint BEM for regularization of problems with improper boundary conditions. J Soft Comput Civ Eng 2018;2(2):01-18. <https://doi.org/10.22115/scce.2018.108597.1036>.

2588-2872/ © 2018 The Authors. Published by Pouyan Press.

This is an open access article under the CC BY license (<http://creativecommons.org/licenses/by/4.0/>).



1. Introduction and background

Discontinuum mechanics govern a class of problems where the materials involved are, in general, granular in nature or particulates, e.g., aggregates, noncohesive soils, aerosols, and atmospheric pollutants, among others. The numerical modeling of such problems is largely based on the modeling of the contact mechanics among material granules and is of common interest in many sciences and engineering fields. The complexity of the particle interaction in such models cannot be realistically represented by continuum-based models, such as the Finite Element Method (FEM) and the Boundary Element Method (BEM). The Discrete Element Method (DEM) is a discontinuum mechanics based method that finds its roots in the 1979 pioneering work of Cundall and Strack [1] who reported on a 2-D method for modeling granular material. The individual particles are customarily represented by simple shapes that move in space as rigid bodies. Despite the rigid particle assumption, the original form of the DEM estimates the particle-to-particle contact forces based on deformable particle interaction laws. The majority of analytical solutions that estimate the contact forces are developed from Hertzian theory. Such solutions exist only for a few simple shapes of the contact area (e.g. circles and triangles), and a review of particle interaction laws is reported in [2]. Alternatively, Mathews [3] considered deformable particles in a system that move and interact with each other and the system boundaries (if any) under the action of contact and field (non-contact) forces. The motion of the particles is governed by Newton's equations of motion that are solved in a time-marching fashion within the DEM framework while the particle kinematic interaction forces using a quasi-static approach using an elastostatic BEM [3]. For the purposes of this work in problems considered with the proposed DEM-BEM method, bodies are set in an empty space which doesn't contain any external supports. Under these conditions, if displacement or force acts on a body, the latter will develop rigid body modes. In the proposed DEM-BEM method an elastostatic BEM is used, where, it is required that all bodies are self-equilibrated and properly constrained against rigid body motion. In classical BEM formulations, however, the constraints are applied on the boundary of the solution domain. If such constraints do not stem from the physical realization of the problem, they tend to alter the deformation response of the body. Furthermore, it is often necessary that the boundary of a body remains unconstrained for the model to accommodate traction only boundary conditions [3].

The role of rigid body modes in the BEM is studied by Vable [4], where, the ways in which rigid body motion appears in BEM solutions is discussed and an algorithm to eliminate rigid body motion by modifying input data is presented. The necessary modifications are determined by subjecting a body to a unit rigid body motion at each boundary support and computing the corresponding unknown traction fields. These tractions are then used to calculate the displacement that needs to be "subtracted" from the input data to account for the rigid body motion that would have occurred in the originally considered problem. Some of the variables needed for this computation have to be determined from analysis for matrix conditioning improvement. The use of Vable's algorithm requires several additional computations before a BEM system is ready to be solved.

Blázquez et al. [5] and Vodička et al. [6,7] present modifications to the Boundary Integral Equation (BIE) to account for rigid body motion through two main approaches: a) adding boundary point supports (“Method S”) and b) adding integral operator(s) based on Fredholm Theory [8] to the BIE (“Method F”). It is concluded that “Method S” gives acceptable results for problems with equilibrated loading conditions, but is not well suited for complex loading scenarios. Furthermore, the use of “Method S” does not allow for unconstrained boundaries. “Method F” approaches have been studied by several researchers as discussed in [9], and are based on incorporating Fredholm Integral Operators into the BIE such that invertible system matrices are obtained. Employment of Method F requires the use of additional variables that have to be selected based on several matrix invertibility conditions.

Asadollahi and Tonon [9] use an elastostatic BEM to analyze rock block systems which have no naturally occurring boundary supports. Rock block systems are composed of a rock block surrounded on all sides by a mass of rock. The BEM is employed to compute the deformation of the rock block due to an all-encompassing traction field caused by the surrounding rock mass. Each face of the block is discretized by several triangular elements and rigid body translation is eliminated by fixing one arbitrary boundary node. Since only one boundary node is fixed, the system matrices should still be singular due to rigid body rotations. It is stated, however, that due to round off errors the system matrices are ill-conditioned and a matrix inverse can be found using the algorithm presented in [10]. This method of eliminating rigid body modes is suitable for the rock block systems analyzed in, [9] since, all tractions are known before the BEM solver is employed. This method is not applicable, however, to bodies with unconstrained boundaries.

The removal of rigid body motion has also been examined using several other mathematical approaches including “Regularization” [11,12], “Singular Value Decomposition” [13], and “Algebraic Multigrid Methods” [14] among others. An overview of these methods is given in [9,15]. In general, as stated in [9], the fundamental concepts of these mathematical approach based methods are difficult to interpret from an engineering point of view. For problems where the boundary of a body should remain unconstrained, or partially constrained, while the body is subjected to a set of unbalanced forces, a BEM method is required where rigid body modes can be eliminated through internal constraints. In standard elastostatic BEM procedures, a discretized BIE is solved to obtain all unknown displacements and tractions on a boundary, after which, Somigliana’s Identity [16] is employed in a post-processing fashion to compute interior displacements. It is evident that interior points cannot be fixed using this solution methodology, and there is a relatively limited amount of literature on applying internal constraints in the BEM. Mina and Rashed [17] use the BEM to model floor slabs that are supported in the interior by columns. In this work point collocation equations are expressed for each column and solved simultaneously with the governing BIE. The governing equation and corresponding fundamental solutions used in [17], however, are based on plate bending theory which is different from elastostatics. In addition, the systems considered by Mina and Rashed are only loaded in one direction that is out of a plane with respect to the floor slabs.

This work proposes an Interior-Constraint BEM where rigid body modes are eliminated by constraining points within the domain of a body. The methodology of the proposed work is

presented with respect to an elastostatic BEM formulation. The application to potential problems is a straightforward reduction on the number of constraints. It is expected that an unknown reactive force field, equivalent to a body force, will develop when interior points or regions are constrained. Subsequently, three approaches for enforcing interior constraints are presented and discussed in detail. The first approach assumes that the equivalent force is a concentrated force that develops at the constrained degree of freedom. The next approach assumes that a finite region is constrained and body forces develop over the finite region. The third approach assumes that the displacements at selected interior points are constrained, and the equivalent smooth body force distributions are assumed over the entire body. The proposed method is evaluated through assessment and verification studies where it is compared to analytical and Finite Element Method (FEM) solutions.

2. Methodology

2.1. 2D Elastostatic BEM formulation

Consider the 2D linear elastic, homogenous, isotropic body Ω bounded by Γ with outward normal \mathbf{n} shown in Fig. 1. Assuming plane strain conditions and small deformations the governing equation is the Lamé-Navier equation expressed in indicial notation as [18].

$$\left(\frac{1}{1-2\nu}\right)u_{j,ji} + u_{i,jj} + \frac{1}{\mu}b_i = 0 \quad (1)$$

where u is the displacement field at any point, b is body force per unit mass, $i, j = 1, 2$ denote directions along the global Cartesian coordinate system with unit vectors $\mathbf{e}_1, \mathbf{e}_2$, ν = Poisson's ratio, and μ = Lamé's Constant.

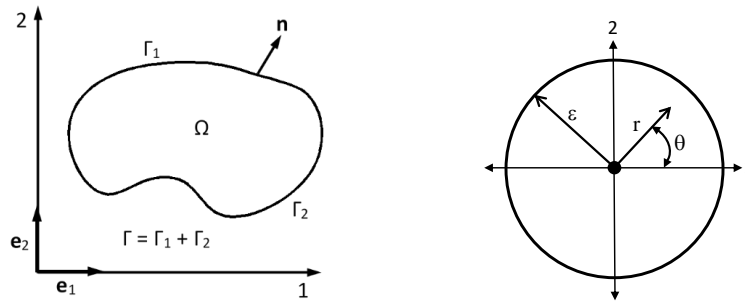


Fig. 1. 2-D Elastic Body: Nomenclature.

The associated boundary conditions are expressed as [19],

$$u_i = \bar{u}_i \quad \text{on } \Gamma_1 \quad (3)$$

$$t_i = \sigma_{ij}n_j = \bar{t}_i \quad \text{on } \Gamma_2 \quad (4)$$

where $\Gamma_1 \cup \Gamma_2 = \Gamma$, \bar{u}_i and \bar{t}_i are prescribed displacements and tractions on boundary segments Γ_1 and Γ_2 respectively, σ_{ij} is the stress field, and n_j is the component in direction j of the outward

normal to the boundary. The associated BIE is developed through well established procedures [19], and is expressed as:

$$c_{ij}^q u_j^q + \int_{\Gamma} t_{ij}^* u_j d\Gamma = \int_{\Gamma} u_{ij}^* t_j d\Gamma + \int_{\Omega} u_{ij}^* b_j d\Omega \quad (5)$$

where: (i) u_j and t_j represent the j component of boundary displacement and traction fields, respectively, (ii) b_j represents the body force components, (iii) “ q ” is a point on the boundary, (iv) c_{ij}^q is the Cauchy Principal Value [20] at point “ q ” commonly referred to as the jump term [19], and (v) u_{ij}^* , t_{ij}^* are the fundamental solutions (Green’s Functions) for displacements and tractions, respectively. The fundamental solutions are defined between any two points in the solution domain expressed in indicial notation as [21]:

$$u_{ij}^* = \frac{1}{8\pi\mu(1-\nu)} \left[(3 - 4\nu) \ln\left(\frac{1}{r}\right) \delta_{ij} + \mathbf{r}_{,i} \mathbf{r}_{,j} \right] \quad (6)$$

$$t_{ij}^* = \frac{1}{4\pi(1-\nu)r} \left[\frac{\partial \mathbf{r}}{\partial \mathbf{n}} \{ (1 - 2\nu) \delta_{ij} + 2\mathbf{r}_{,i} \mathbf{r}_{,j} \} + (1 - 2\nu) (n_i \mathbf{r}_{,j} - n_k \mathbf{r}_{,i}) \right] \quad (7)$$

where \mathbf{r} is the distance vector between the two points, and δ_{ij} is the Kronecker delta function [22]. The BIE can be expressed in a discrete form through a collocation approach [19]. The discretization yields N boundary degrees of freedom (DOF) and M domain DOF. The BIE Eq. (5) is cast then in a matrix form as:

$$\mathbf{Hu} = \mathbf{Gt} + \mathbf{Bb} \quad (8)$$

Where: (i) \mathbf{H} and \mathbf{G} are $N \times N$ influence matrices associated with displacements, \mathbf{u} , and tractions, \mathbf{t} , on the boundary nodes, respectively, and are computed based on a collocation approach from integrals of the fundamental solutions over the boundary of the domain; (ii) \mathbf{B} is an $N \times M$ influence matrix associated with the body forces, and is computed based on a collocation approach from the last integral, $\int_{\Omega} u_{ij}^* b_j d\Omega$, of the BIE Eq. (5); and (iii) \mathbf{b} are the discrete nodal body forces. Once the BIE is solved, displacements, u^{q_i} , at points q_i within the domain can be found using Somigliana’s identity [18] which is expressed in a matrix form as [19]:

$$\mathbf{u}^{q_i} + \tilde{\mathbf{H}}\mathbf{U} = \tilde{\mathbf{G}}\mathbf{T} + \tilde{\mathbf{B}}\mathbf{b} \quad (9)$$

where $\tilde{\mathbf{H}}$ and $\tilde{\mathbf{G}}$ are matrices of dimension $M \times N$ that contain the integration of the fundamental solutions over the boundary with respect to point q_i , and $\tilde{\mathbf{B}}$ is a matrix of dimension $M \times M$ that contains the integration of the displacement fundamental solution Eq. (6), over each domain element with respect to point q_i and involves only interior points. Details on the evaluation of the submatrices in Eqs (8) and (9) and the implementation of the BEM method are widely available in the literature, e.g. [19,22].

2.2. Interior-constraint BEM formulation

The proposed Interior-Constraint BEM (ICBEM) of this work eliminates rigid body motion in a deformable body by constraining displacements at interior points. This is achieved by simultaneously casting the governing BIE (Eq. (8)) and Somigliana's Identity (Eq. (9)) in a matrix form as:

$$\begin{bmatrix} \mathbf{H} & -\mathbf{B} \\ \tilde{\mathbf{H}} & -\tilde{\mathbf{B}} \end{bmatrix} \begin{Bmatrix} \mathbf{u} \\ \mathbf{b} \end{Bmatrix} = \begin{bmatrix} \mathbf{G} & \mathbf{0} \\ \tilde{\mathbf{G}} & -\mathbf{I} \end{bmatrix} \begin{Bmatrix} \mathbf{t} \\ \mathbf{u}^{q_i} \end{Bmatrix} \quad (10)$$

Subsequently, and in view of the physics of the real problem, a number of interior points, q_i , are selected at which the necessary displacement constraints, e.g. $\mathbf{u}^{q_i} = \mathbf{0}$, should be attained. The problem then reduces to computing the associated equivalent body force field, b^{eq} , that, along with the boundary excitations and other existing body forces, will satisfy these constraint conditions. Without loss of generality, it is assumed that other existing body forces are zero and, therefore, in Eq. (10) $\mathbf{b} = \mathbf{b}^{eq}$ represents a discrete form of the equivalent body forces. It is evident that the discrete form depends on the spatial distribution of the body force. In this work three cases have been considered and investigated: (a) The first case assumes that at every constrained interior DOF an equivalent concentrated body force develops; (b) The second case assumes that a finite, yet small, area in the domain is constrained and all equivalent body forces are distributed over this area; and (c) an appropriate number of DOF at interior points are constrained and the equivalent body forces are assumed to be distributed over the entire domain. As discussed in the following sections the case of concentrated body force leads to strong singularities and a solution cannot be obtained, while the other two cases lead to stable and accurate solutions where equilibrium is satisfied.

2.2.1. Concentrated equivalent body forces

The case of concentrated body forces (i.e., body force distribution is a delta function) is considered first to demonstrate that this option leads to singular integral values. When a single interior point is constrained the body force term of the BIE (Eq. (5)) becomes unbounded. This is demonstrated by considering the computation of the body force term with respect to the circular area shown in Fig. 1 when loaded by a constant body force, i.e.

$$\int_{\Omega} u_{ij}^* b_j d\Omega = \frac{1}{8\pi\mu(1-\nu)} \int_0^\varepsilon \int_0^{2\pi} \left[(3-4\nu) \ln\left(\frac{1}{r}\right) \delta_{ij} + \mathbf{r}_i \mathbf{r}_j \right] \frac{F}{2\pi\varepsilon} d\theta dr \quad (11)$$

Where r and θ are the radial and angular coordinates and the resultant body force (R_b) acting over the circle is expressed in terms of the constant F as

$$R_b = \int_0^\varepsilon \int_0^{2\pi} \frac{F}{2\pi\varepsilon} d\theta dr = F \quad (12)$$

When $\varepsilon \rightarrow 0$, Eq. (11) is equivalent to computing the body force term with respect to a single point, i.e.

$$\int_{\Omega} u_{ij}^* b_j d\Omega = \frac{F}{16\pi^2\mu(1-\nu)} \lim_{\varepsilon \rightarrow 0} \left\{ \int_0^\varepsilon \int_0^{2\pi} \left[(3-4\nu) \ln\left(\frac{1}{r}\right) \delta_{ij} + \mathbf{r}_i \mathbf{r}_j \right] \frac{1}{\varepsilon} d\theta dr \right\} \quad (13)$$

The derivative terms in Eq. (13) are non-singular and can be evaluated without any issues. Evaluating the other terms in Eq. (13) the following expression is obtained when $i = j$:

$$\frac{(3-4\nu)F}{16\pi^2\mu(1-\nu)} \lim_{\varepsilon \rightarrow 0} \left\{ \int_0^\varepsilon \int_0^{2\pi} \left[\ln\left(\frac{1}{r}\right) \delta_{ij} \right] \frac{1}{\varepsilon} d\theta dr \right\} = \frac{(3-4\nu)F}{8\pi\mu(1-\nu)} \lim_{\varepsilon \rightarrow 0} \left\{ 1 + \ln\left(\frac{1}{\varepsilon}\right) \right\} \quad (14)$$

It is evident that Eq. (14) does not converge to a finite value when ε approaches zero. The same analysis of computing the body force term over a single point has also been considered for linear, polynomial, and exponential body force distributions. In all cases obtaining a non-singular solution is not feasible. Special Gauss Integration schemes (e.g. [23]) which are often employed in the BEM to treat singular integration over boundary elements cannot be used to evaluate the integrals in Eq. (14), since, the area of integration tends to zero. There are some mathematically based approaches for approximating divergent integrals by eliminating terms that tend towards infinity such as Hadamard Regularization [24], but this is beyond the scope of this work since it increases the complexity of the computations. It is therefore concluded that in the ICBEM all body forces need to be distributed over a finite area, as discussed in the following two sections.

2.2.2. Body forces distributed over a small, finite area

This approach assumes that a finite, yet small, area in the domain is constrained and all equivalent body forces are distributed over this area. In this work, the constrained area is a Triangular Region (TR), as shown in Fig. 2. The displacements at the TR vertices are constrained, $\mathbf{u}^{qi} = \mathbf{0}$, and the boundary is discretized with quadratic line elements. The discrete body force vector \mathbf{b} in Eq. (10) consists of values of the body force at the triangle vertices. The TR is sized in such a way that its effect on body stiffness is negligible, and this is demonstrated in the Assessment and Verification Studies section.

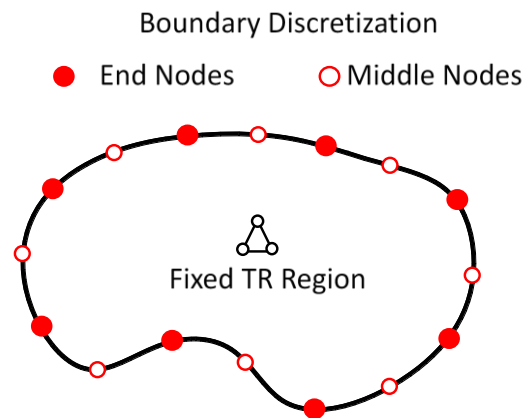


Fig. 2. ICBEM discretization for body forces distributed over a finite region.

2.2.3. Body forces distributed over the entire domain

In this approach, in order to remove the two translational and one rotational rigid body modes, two interior points are defined first. The first interior point, point “c”, is typically placed, without loss of generality, at the body’s center of gravity and the second point, point “o”, is placed at an offset distance from point “c” in any direction, as shown in Fig 3a. The displacements $\mathbf{u}^c = \{u_1^c \quad u_2^c\}^T$ at point “c”, shown in Fig. 3b, are set to zero to constrain rigid body translation. The

associated body force field, $\mathbf{b}^{\text{tr}} = \{b_1^{\text{tr}} \ b_2^{\text{tr}}\}^T$, is assumed uniformly distributed over the entire domain as shown in Fig. 3a, where, “tr” denotes that the body forces are associated with the translational constraints at point “c”. Rigid body rotation is constrained by restraining the displacement at an additional interior point “o” in a direction perpendicular to a line that passes through “c” and “o, as shown in Fig 3c”. In the implementation of the method in this work, and without loss of generality, point “o” is offset horizontally from point “c”. Consequently, to constrain rigid body rotation the vertical displacement, u_2^o at point “o” must be constrained. To develop the ensuing internal moment from constraining rigid body rotation, a rotational body force field, b^r , with a linear distribution over the entire domain about point “c” is assumed, as shown in Fig. 3a.

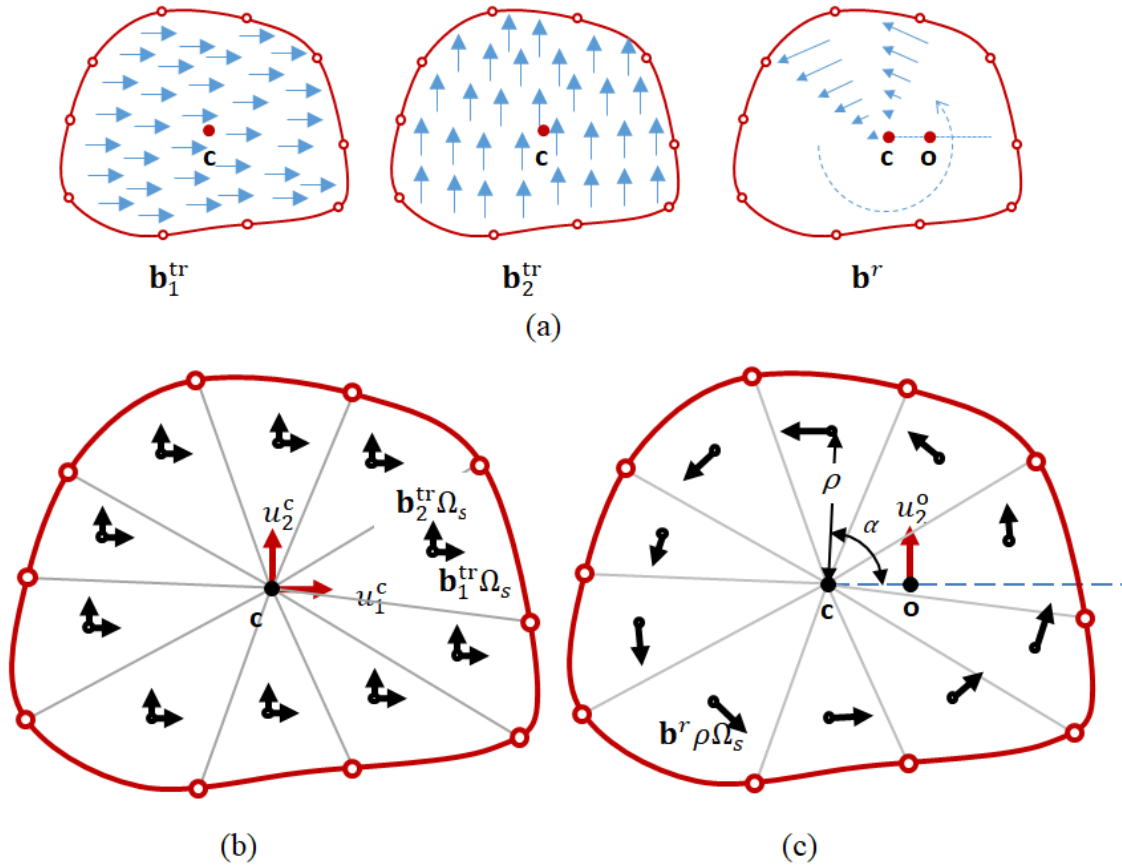


Fig. 3. ICBEM methodology for body forces distributed over entire domain: (a) Body force fields, (b) Translational constraints, (c) Rotational constraint.

Introducing the displacements u_1^c, u_2^c , and u_2^o and the associated body force fields $b_1^{\text{tr}}, b_2^{\text{tr}}$, and b^r in the ICBEM Eq. (10), the latter becomes:

$$\begin{bmatrix} \mathbf{H} & -\mathbf{B} & -\mathbf{B}^r \\ \tilde{\mathbf{H}}^c & -\tilde{\mathbf{B}}^{\text{tr},c} & -\tilde{\mathbf{B}}^{r,c} \\ \tilde{\mathbf{H}}^o & -\tilde{\mathbf{B}}^{\text{tr},o} & -\tilde{\mathbf{B}}^{r,o} \end{bmatrix} \begin{Bmatrix} \mathbf{U} \\ \mathbf{b}^{\text{tr}} \\ b^r \end{Bmatrix} = \begin{bmatrix} \mathbf{G} & \mathbf{0} & \mathbf{0} \\ \tilde{\mathbf{G}}^c & -\mathbf{I} & \mathbf{0} \\ \tilde{\mathbf{G}}^o & \mathbf{0} & -1 \end{bmatrix} \begin{Bmatrix} \mathbf{U} \\ \mathbf{u}^{\text{tr}} \\ u_2^o \end{Bmatrix} \quad (15)$$

where: (i) the first equations are the discrete BIE, (ii) the middle equations are Somigliana's Identity for the constrained displacements, \mathbf{u}^c , at point "c", and (iii) the last equation is Somigliana's Identity for the constrained displacement, u_2^o , at point "o". Matrices $\tilde{\mathbf{G}}^c$, $\tilde{\mathbf{H}}^c$, $\tilde{\mathbf{G}}^o$ and $\tilde{\mathbf{H}}^o$, are the $\tilde{\mathbf{H}}$ and $\tilde{\mathbf{G}}$ matrices defined in Eq. (10) and evaluated with respect to internal points "c" and "o", respectively. Matrices $\tilde{\mathbf{B}}^{\text{tr},c}$ and $\tilde{\mathbf{B}}^{\text{tr},o}$ are of size 2 x 2 and 2 x 1, respectively, and matrices $\tilde{\mathbf{B}}^{\text{r},c}$ and $\tilde{\mathbf{B}}^{\text{r},o}$ are of size 1 x 2 and 2 x 1, respectively and are defined based on the body force term in Eq. (5) where the displacement fundamental solution is evaluated with respect to points "c" and "o", as discussed next.

2.2.3.1. Numerical evaluation

The evaluation of these terms requires integration over the domain of interest; however, a discretization of the domain is not necessary. Instead, the domain is divided into triangular regions, as shown in Fig. 3b and 3c that represent convenient, simple areas over which Gaussian quadrature can be applied. Each triangular region is defined by point "c" and two consecutive boundary nodes. In general, the most suitable physical representation of a problem is achieved by placing point "c" at a body's center of gravity, and this is done for all problems in this work. In addition, for this work, each triangular region is defined by one integration point located at the centroid of the region area.

In view of the assumption that the equivalent body forces associated to translational constraints are uniformly distributed, the elements $\tilde{B}_{ij}^{\text{tr}}$ in matrices $\tilde{\mathbf{B}}^{\text{tr},c}$ and $\tilde{\mathbf{B}}^{\text{tr},o}$ are evaluated numerically as:

$$\int_{\Omega} u_{ij}^* b_j d\Omega = \sum_{s=1}^{\# \text{Triangles}} \left\{ \int_{\Omega_s} u_{ij}^* d\Omega_s \right\} b_j^{\text{tr}} = \tilde{B}_{ij}^{\text{tr}} b_j^{\text{tr}} \quad (16)$$

where Ω_s is the area of a triangular region. For the one point, Gauss quadrature employed in this work, Eq. (16) the $\tilde{B}_{ij}^{\text{tr}}$ terms are evaluated as:

$$\tilde{B}_{ij}^{\text{tr}} = \sum_{s=1}^{\# \text{Triangles}} u_{ij}^* \Omega_s \quad (17)$$

Where u_{ij}^* is shown in Eq. (5) for a distance vector defined between points: (i) "c" and the centroid of each triangle for the $\tilde{\mathbf{B}}^{\text{tr},c}$ term, and (ii) points "o" and the centroid of each triangle for the $\tilde{\mathbf{B}}^{\text{tr},o}$ term.

In view of the linear distribution of the equivalent rotational body force, b^r , the latter is written in vector form as

$$\mathbf{b}^r = -[b^r \varrho \sin a] \mathbf{e}_1 + [b^r \varrho \cos a] \mathbf{e}_2 \quad (18)$$

Where: (i) b^r is the magnitude of the rotational body force field, and (ii) a is the angle (measured counter-clockwise) between the horizontal, and a distance vector with magnitude ϱ that is defined from point "c" to the integration point of each triangular region (depicted in Fig. 3c). In a

manner similar to the evaluation of matrices $\tilde{\mathbf{B}}^{\text{tr},c}$ and $\tilde{\mathbf{B}}^{\text{tr},o}$, the elements \tilde{B}_i^r in matrices $\tilde{\mathbf{B}}^{\text{tr},c}$, and $\tilde{\mathbf{B}}^{\text{tr},o}$ can now be expressed in terms of one point Gauss quadrature as

$$\tilde{B}_i^r = \sum_{s=1}^{\# \text{Triangles}} (-u_{i1}^* \sin a + u_{i2}^* \cos a) \rho \Omega_s \quad (19)$$

Finally, matrix \mathbf{B}^r accounts for the effects of the rotational body force field in the BIE and is computed in the same way as Eqs. (19), but the source points correspond to boundary nodes instead of the constrained domain points “c” and “o”. The BEM system matrix is square with dimension $N+3 \times N+3$. The solution to Eq. (15) will yield all unknown field variables, after which, the equilibrium of a body can be verified with the following equations

$$b_i^{\text{tr}} \Omega + F_i = 0 \quad (20)$$

$$\sum_{s=1}^{\# \text{Triangles}} b^r \rho^2 \Omega_s + M = 0 \quad (21)$$

Where F_1 , and F_2 is the resultant external force on the body in the 1, 2 directions, respectively, and M is the total external moment applied on the body about an axis that is orthogonal to the 1, 2 directions.

3. Assessment and verification studies

To assess the proposed ICBE method, it is examined through showcase problems and parametric studies where it is compared to other solution methods. In this section the two variations of the ICBE method will be denoted as methods: (i) M1 – Rigid body motion is constrained by fixing a single domain region, TR as discussed in section 2.2.2, and (ii) M2 – Rigid body motion is constrained by fixing a combination of degrees of freedom at two domain points, and body forces are distributed over the entire domain (section 2.2.3). The following studies are performed:

- (i) Methods M1, M2 are employed to solve the problem of a steel plate symmetrically deformed in tension. In this study, the ICBE method is compared to a known analytical solution and the FEM.
- (ii) Methods M1, M2 are further studied by reconsidering the steel plate problem with an asymmetrically applied displacement field, where, no analytical solution exists for this set of boundary conditions.
- (iii) A parametric study is conducted to assess the effects of the size of the constrained region, TR, with method M1. This study is performed considering the steel plate problem in the preceding study.
- (iv) Methods M1, M2 are employed to solve the steel plate problem when loaded by a traction field which produces an external moment. The accuracy of the ICBE method is assessed by examining plate deformations and through force and moment equilibrium.

3.1. Steel plate deformed in tension

The 2m x 1m steel plate shown in Fig. 4 is deformed in tension on both sides by $u = 0.001$ m. The plate material has a modulus of elasticity $E = 200,000$ MPa, and Poisson's ratio $\nu = 0.25$. The boundary mesh used for methods M1, M2 is shown in Fig. 4(a), where the perimeter is discretized in 120 quadratic boundary elements. The triangle at the center of the plate represents the fixed TR area employed in method M1. For this initial study, the area of the triangle is $A_{\Delta} = 0.0015$ m² which corresponds to 1/1333.33 of the area of the plate. In method M2 for domain integration, there are 2 triangular regions for each quadratic boundary element which corresponds to 240 triangular regions in total. Point "c" in method M2 is placed at the center of the plate, and point "o" is offset 0.05 m to the right of point "c". The problem is also solved by a plain strain FEM analysis (performed with ABAQUS [25]) that is designed to simulate the physics of the model solved with method M1. To this end, a TR area is fixed at the center of the plate in the FEM analysis, and the nodes of this element are denoted by the yellow circles of the FEM mesh shown in Fig. 4(b). The solution obtained from this FEM analysis is denoted as FEM1. It can be seen that even for a simple geometry a much finer mesh is required in the FEM than with the ICBEM. The deformation of the plate (scaled up by 1000) from the ICBEM and FEM solutions are shown in Fig. 4(c). It can be seen that the deformation is almost identical between methods M1, M2 and FEM1. In addition the deformation matches the physical behavior of a plate pulled in tension. It is observed that no significant deformations are introduced by the presence of a fixed TR area in method M1.

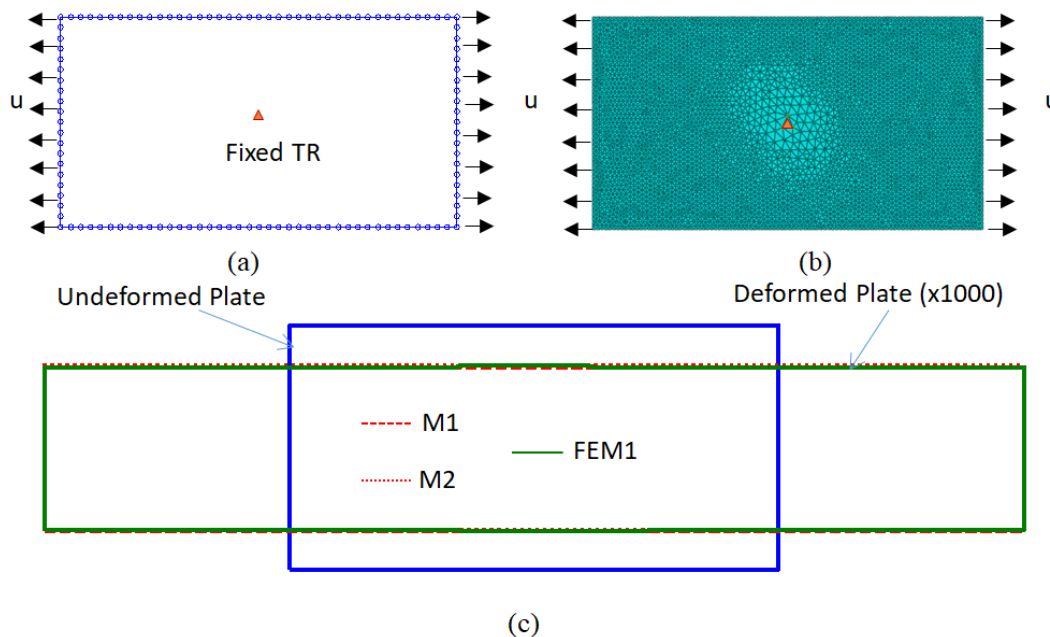


Fig. 4. Steel plate deformed in uniaxial tension: (a) ICBEM Mesh, (b) FEM Mesh (c) Deformed configurations as obtained by M1, M2, and FEM solutions.

The magnitude of the resultant horizontal force on the left side of the plate has been computed with all methods and is reported as *Case 1* in Table 1. The force in Table 1 is compared to the theoretical solution for plain strain conditions [26], i.e.

$$F_{pl} = \sigma_1 A_P = \frac{E}{(1+\nu)(1-2\nu)} \left[(1-\nu) - \frac{\nu^2}{1-\nu} \right] \varepsilon_1 A_P \quad (22)$$

where σ_1 , ε_1 are the stress and strain, respectively, in the horizontal direction on the left side of the plate, and A_P denotes the plate cross sectional area. The percent difference between all methods is negligible at less than 1%.

Table 1

End Force Comparison Study.

Method	F_{pl} (MN)
M1	212.91
FEM1	213.81
M2	212.52
Eq. 22	213.33

To verify that rigid body motion has been constrained by the ICBEM, displacements at the fixed domain points have been back-calculated using Somigliana's Identity for methods M1, M2. These computed displacements are on the order of $1 \times 10^{-19} \approx 0$, and this indicates that the plate has been successfully constrained against rigid body motion. In this example, an arbitrarily small value was selected for A_Δ in method M1, but almost identical results are obtained using much smaller TR areas. For example, using $A_\Delta = 1.5 \times 10^{-6} \text{ m}^2$ yields $F_{pl} = 212.54 \text{ MN}$. It will be observed in the forthcoming sections that this is only the case for systems with equilibrated loading conditions. For method M2 the same value of F_{pl} is obtained when point "o" is offset in a variable direction and distance from point "c". The offset of point "o" does however affect the deformation behavior of the plate. To avoid introducing unwanted deformations in method M2, it is recommended that point "o" be placed as close to point c as possible.

3.2. Steel plate with an asymmetrically applied displacement field

The steel plate problem of the previous section is reconsidered with the applied displacement field $u = 0.001\text{m}$ applied on the left side of the plate only and with no other boundary constraints as shown in Fig 5(a). The problem is solved with the ICBEM and FEM methods. In this example two FEM solutions denoted by FEM1, FEM2 are presented, and these solutions correspond to the emulation of methods M1, M2, respectively. For methods M1, M2 and FEM1 the problem setup is the same as in the last section with the exception of the new boundary conditions. In order to obtain solution FEM2 that is consistent with the model that corresponds to M2, it is necessary to load and constrain the plate as shown in Fig. 5(b). In this case, the plate is loaded with the body force field \mathbf{b}^{tr} obtained from the method M2 solution, and the left end of the plate is constrained against horizontal displacement. In addition, the mid-point of the left end is constrained against vertical displacement to ensure that all rigid body modes are accounted for. Figure 5(c) shows the plate deformation, where it can be seen that the physical behavior of methods M1 and FEM1 are significantly different than that of methods M2 and FEM2.

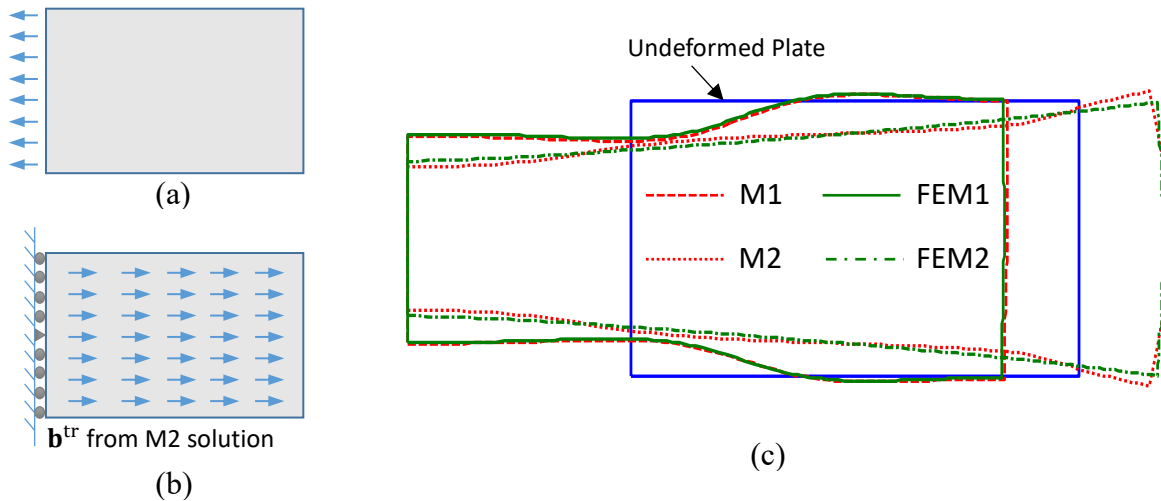


Fig. 5. Steel plate in asymmetric deformation: (a) Induced deformation for M1, M2, and FEM1 solutions; (b) Boundary conditions for FEM2 model only, (c) Deformed configurations as obtained by all methods.

As expected the deformations from methods M1 and M2 are almost identical to their counterpart solutions FEM1 and FEM2, respectively. In methods M1 and FEM1 the deformation is non-uniform, whereas, for methods M2, FEM2 the plate deforms in a uniform tapered manner. For methods M1, FEM1 the deformation is localized about the constrained domain region over which all body forces are distributed. For methods M2, FEM2 the plate deformation is uniformly tapered in the horizontal direction which is analogous to the distribution of the uniform body force field \mathbf{b}^{tr} over the entire domain. The deformations obtained from both ICBEM formulations are accurate within the assumption of how body forces are distributed over the domain. The magnitude of the resultant horizontal force on the left side of the plate has been computed for all methods and is reported in Table 2.

Table 2

End Force Comparison Study.

Method	F_{pl} (MN)
M1	140.41
FEM1	138.15
M2	291.80
FEM2	289.10

It should be noted that this force cannot be computed analytically with respect to the loading condition of the plate. As expected the difference in force is negligible between methods M1, M2 and their counterpart finite element solutions FEM1, FEM2, respectively. There is a significant difference in force between methods M1 and M2, and this is attributed to the difference in assumed body force distributions of the two approaches. The force from method M2 is notably larger than in method M1, since, in method M2 the body forces are distributed over a significantly larger area than in method M1. The displacements at the fixed domain points in methods M1, M2 have been back-calculated and again are on the order of $1 \times 10^{-19} \approx 0$ indicating that rigid body motion has been eliminated. Using a notably smaller triangle size of $A_{\Delta} = 1.5 \times 10^{-7}$

6 m^2 in method M1 yields $F_{pl} = 85.43 \text{ MN}$. It can be seen that this force does not match the values reported in Table 2, and a correlation between A_{Δ} and F_{pl} is evident. This correlation is studied in the next section.

3.3. Method M1 – Parametric Study

To further study the ICBEEM the selection of A_{Δ} in method M1, is examined through a parametric study. The steel plate problem with the unbalanced load shown in Fig 5(a) in the previous section 3.2 is chosen for the parametric study since the resultant force on the fixed TR will be different than zero. The plate boundary is discretized into 120 boundary elements, however, the area of the fixed TR varies from $A_{\Delta} = 1 \times 10^{-4} \text{ m}^2 - 0.02 \text{ m}^2$, representing 0.005 % - 1% of the plate area. For comparison, the finite element solution FEM1 (see sections 3.1 – 3.2) is also computed for all A_{Δ} . In all solutions, the magnitude of the horizontal component of the resultant force, F_{pl} , on the left side of the plate is computed. In addition, a FEM solution is obtained for a reference problem. In this case, the plate is fixed at a single point at its center against translations. The reference problem represents the limiting case where the constrained area TR approaches zero in the M1 and FEM1 solutions. The horizontal component of the resultant force on the left side, F_o , is determined and assumed the reference solution. The findings are summarized in a graph form that relates the normalized force F_{pl}/F_o to the normalized area A_p/A_{Δ} and is shown in Fig 6. It is observed that M1 and FEM1 solutions agree well for the all areas considered. It is evident that the convergence to the reference solution is inversely proportional to the size of A_{Δ} , since the rigid TR area affects the stiffness of the plate. Larger areas introduce errors while extremely small areas may lead to instabilities due to roundoff errors. As a rule of thumb the size of A_{Δ} should be selected in the range 0.001 % to 0.01% of the area of the domain to ensure that: (i) The rigidity of the fixed TR area does not affect the stiffness of the domain and (ii) the fixed TR area is large enough that its effect can be numerically accounted for in method M1.

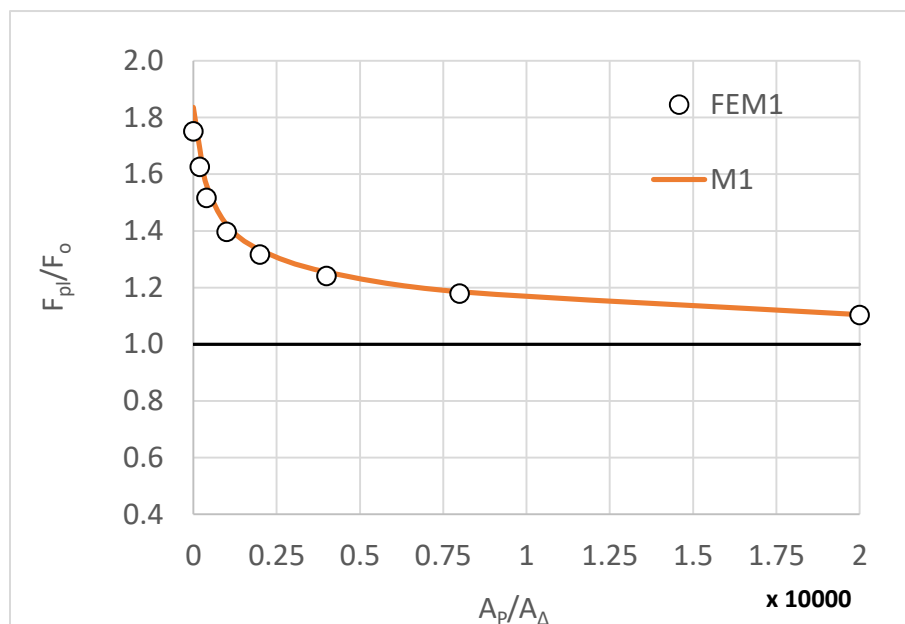


Fig. 6. Method M1 – Effects of fixed TR size on force solution.

3.4. Steel plate loaded with traction field that produces a moment

For this study, the steel plate problem is reconsidered when loaded by the traction field $t = 324$ MN/m shown in Fig. 7(a). This problem is solved with methods M1 and M2. The deformation of the plate for both methods is shown in Fig. 7(b)-(d). For method M1 when A_P/A_Δ is selected within the minimum and maximum limits established in the last section the plate deforms as shown in Fig. 7(b). It can be seen that this deformed configuration resembles a rigid body rotation and is not representative of the loading condition. The plate is in force equilibrium, and the displacements at the fixed TR area are on the order of 1×10^{-16} indicating that rigid body motion has been constrained. It appears, however, that the plate does not properly develop the external moment produced by the traction field for a selection of A_P/A_Δ within the established limits. To help develop the moment the problem is reconsidered using method M1 with two fixed TR areas. The additional fixed TR area is offset to the right of the original fixed TR area (at the center of the plate) by 0.2 m. The corresponding deformed configuration is shown in Fig. 7(c) where it is compared to a solution from method M2 shown in Fig. 7(d). The deformations are fairly similar in behavior but differ in magnitude. The localized deformations in the plate due to the traction field can clearly be seen in method M2. It can be seen that the deformation is representative of the applied traction field, and the plate undergoes both translational and rotational deformations which indicates that no rigid body motion occurred. For method M1 the deformation still largely resembles a rigid body rotation. It is concluded that method M1 is better suited for applications where rigid body rotations are expected to remain small. In method M2 the external moment is balanced by the rotational body force field \mathbf{b}^F (Eq. (21)).

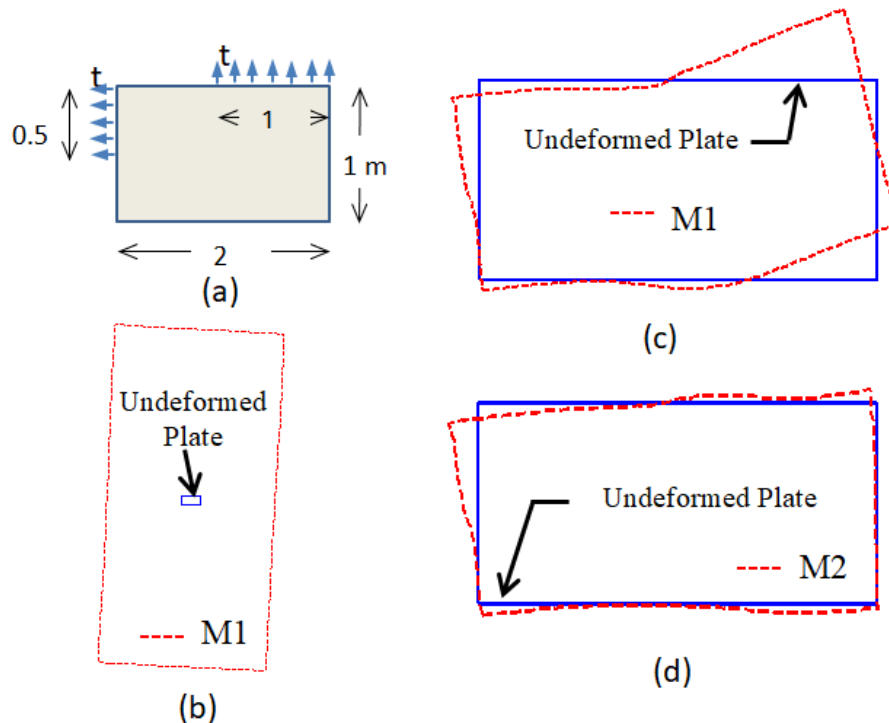


Fig. 7. Deformation of steel plate with applied traction field: (a) Plate loading; (b) Method M1 for A_P / A_Δ between minimum and maximum limits; (c) Method M1 with two TR; (d) Method M2.

Force and moment equilibrium for the plate have been verified using Eqs. (20) – (21) and the results are reported in Table 3. It can be seen that the internal forces and moment obtained from the integration of body forces are equal and opposite to the external forces and moment obtained from the integration of tractions. The residual forces and moments are negligible, as shown in the last row of the table, verifying, thus, that the body is in equilibrium.

Table 3

Verification of Plate Equilibrium.

	F₁ (MN)	F₂ (MN)	M (MN-m)
External Forces <i>Traction Integration</i>	-167.400	329.400	206.550
Internal Forces <i>Body Force Integration</i>	167.448	-329.398	-206.59
Residual Forces	0.048	0.002	-0.040

4. Conclusions

This work discussed in detail the development of an Interior-Constraint BEM (ICBEM) for regularization of elastostatic problems with improper boundary conditions, which in general, exhibit rigid body motion. The regularization process generates an unknown reactive force field due to the imposed interior constraints that is equivalent to a body force field. Three assumptions related to the equivalent force field are investigated: (i) a concentrated force develops at a constrained degree of freedom; (ii) the force field is uniformly distributed over a finite, yet small, triangular constrained interior region, method M1; (iii) the displacements at interior degrees of freedom are constrained and the equivalent body forces are distributed over the entire body, method M2. The evaluation of the proposed approaches has shown that:

- a. The assumption of concentrated body forces at discrete constrained degrees of freedom leads to integration singularities and is not valid.
- b. Methods M1 and M2 successfully remove rigid body translations and satisfy static equilibrium.
- c. Both methods have been successfully verified through comparisons with independent solutions based on the Finite Element Methods.
- d. Methods M1 and M2 correspond to solutions of different physical systems.
- e. Method M1 is simpler to implement than method M2.
- f. Method M1 is better suited for applications with rigid body translation only, when a single interior region is constrained. For applications with rigid body rotations a separate interior region needs to be constrained.
- g. The relative size of the constrained interior region in method M1 to the size of the solution domain affects the solution. These effects are more pronounced in the computation of domain forces and less evident in the deformations. Recommendations on the relative size have been established.
- h. Method M2 is shown to be more robust and independent of solution parameters.

References

- [1] Cundall PA, Strack ODL. A discrete numerical model for granular assemblies. *Geotechnique* 1979;29:47–65.
- [2] Poschel T, Schwager T. *Computational Granular Dynamics: Models and Algorithms*. 2005.
- [3] Mathews IV GF. *Developments for the advancement of the discrete element method*. University of South Carolina, 2015.
- [4] Vable M. Importance and use of rigid body mode in boundary element method. *Int J Numer Methods Eng* 1990;29:453–72. doi:10.1002/nme.1620290302.
- [5] BLÁZQUEZ A, MANTIČ V, PARÍS F, CAÑAS J. ON THE REMOVAL OF RIGID BODY MOTIONS IN THE SOLUTION OF ELASTOSTATIC PROBLEMS BY DIRECT BEM. *Int J Numer Methods Eng* 1996;39:4021–38. doi:10.1002/(SICI)1097-0207(19961215)39:23<4021::AID-NME36>3.0.CO;2-Q.
- [6] Vodička R, Mantič V, París F. Note on the removal of rigid body motions in the solution of elastostatic traction boundary value problems by SGBEM. *Eng Anal Bound Elem* 2006;30:790–8. doi:10.1016/j.enganabound.2006.04.002.
- [7] Vodička R, Mantič V, París F. On the removal of the non-uniqueness in the solution of elastostatic problems by symmetric Galerkin BEM. *Int J Numer Methods Eng* 2006;66:1884–912. doi:10.1002/nme.1605.
- [8] Fredholm I. Sur une classe d'équations fonctionnelles. *Acta Math* 1903;27:365–90. doi:10.1007/BF02421317.
- [9] Asadollahi P, Tonon F. Coupling of BEM with a large displacement and rotation algorithm. *Int J Numer Anal Methods Geomech* 2011;35:749–60. doi:10.1002/nag.916.
- [10] Rump SM. Inversion of extremely Ill-conditioned matrices in floating-point. *Jpn J Ind Appl Math* 2009;26:249–77. doi:10.1007/BF03186534.
- [11] Lutz E, Ye W, Mukherjee S. Elimination of rigid body modes from discretized boundary integral equations. *Int J Solids Struct* 1998;35:4427–36. doi:10.1016/S0020-7683(97)00261-8.
- [12] Sapountzakis EJ, Dikaros IC. Advanced 3D beam element of arbitrary composite cross section including generalized warping effects. *Int J Numer Methods Eng* 2015;102:44–78. doi:10.1002/nme.4849.
- [13] Chen JT, Chen WC, Lin SR, Chen IL. Rigid body mode and spurious mode in the dual boundary element formulation for the Laplace problems. *Comput Struct* 2003;81:1395–404. doi:10.1016/S0045-7949(03)00013-0.
- [14] Xiao Y-X, Zhang P, Shu S. An algebraic multigrid method with interpolation reproducing rigid body modes for semi-definite problems in two-dimensional linear elasticity. *J Comput Appl Math* 2007;200:637–52. doi:10.1016/j.cam.2006.01.021.
- [15] Ko YY, Chen CH. Application of symmetric Galerkin boundary element method on elastostatic neumann problems. *Int Assoc Comput Methods Adv Geomech* 2008:146–53.
- [16] Rizzo FJ. An integral equation approach to boundary value problems of classical elastostatics. *Q Appl Math* 1967;25:83–95. doi:10.1090/qam/99907.
- [17] Wagdy M, Rashed YF. Boundary element analysis of multi-thickness shear-deformable slabs without sub-regions. *Eng Anal Bound Elem* 2014;43:86–94. doi:10.1016/j.enganabound.2014.03.011.
- [18] Lamé G. *Leçons sur la théorie mathématique de l'élasticité des corps solides* par G. Lamé. Gauthier-Villars; 1852.

- [19] Brebbia CA, Dominguez J. *Boundary elements: an introductory course*. WIT press; 1994.
- [20] Cauchy AL. *Sur un nouveau genre de calcul analogue au calcul infinitésimal*. Oeuvres Complet d'Augustin Cauchy, Gauthier-Villars, Paris 1826.
- [21] Kelvin, Lord. *Note on the integration of the equations of equilibrium of an elastic solid*. Cambridge Dublin Math J 1848;3:87–9.
- [22] Kronecker L. *Vorlesungen über die Theorie der Determinanten: Erste bis Einundzwanzigste Vorlesungen*. vol. 2. BG Teubner; 1903.
- [23] Mineur H, Berthod-Zaborowski M, Henri B, Jean M. *Techniques de calcul numérique: à l'usage des mathématiciens, astronomes, physiciens et ingénieurs*. Dunod; 1952.
- [24] Hadamard J. *Le problème de Cauchy et les équations aux dérivées partielles linéaires hyperboliques* 1932.
- [25] Dassault. *Abaqus 6.8 Program* 2008.
- [26] Slaughter WS. *Variational Methods. Linearized Theory Elast.*, Boston, MA: Birkhäuser Boston; 2002, p. 387–429. doi:10.1007/978-1-4612-0093-2_10.